7-22-2010

Three-Dimensional Mechanics of Yakutat Convergence in the Southern Alaskan Plate Corner

Peter O. Koons
University of Maine - Main, peter.koons@maine.edu

B. P. Hooks

T. Pavlis

P. Upton

A. D. Barker

Three-dimensional mechanics of Yakutat convergence in the southern Alaskan plate corner

P. O. Koons,[1] B. P. Hooks,[2] T. Pavlis,[2] P. Upton,[1,3] and A. D. Barker[1,4]

Received 11 February 2009; revised 12 January 2010; accepted 20 January 2010; published 22 July 2010.

[1] Three-dimensional numerical models are used to investigate the mechanical evolution of the southern Alaskan plate corner where the Yakutat and the Pacific plates converge on the North American plate. The evolving model plate boundary consists of Convergent, Lateral, and Subduction subboundaries with flow separation of incoming material into upward or downward trajectories forming dual, nonlinear advective thermal/mechanical anomalies that fix the position of major subaerial mountain belts. The model convergent subboundary evolves into two teleconnected orogens: Inlet and Outlet orogens form at locations that correspond with the St. Elias and the Central Alaska Range, respectively, linked to the East by the Lateral boundary. Basins form parallel to the orogens in response to the downward component of velocity associated with subduction. Strain along the Lateral subboundary varies as a function of orogen rheology and magnitude and distribution of erosion. Strain-dependent shear resistance of the plate boundary associated with the shallow subduction zone controls the position of the Inlet orogen. The linkages among these plate boundaries display maximum shear strain rates in the horizontal and vertical planes where the Lateral subboundary joins the Inlet and Outlet orogens. The location of the strain maxima shifts with time as the separation of the Inlet and Outlet orogens increases. The spatiotemporal predictions of the model are consistent with observed exhumation histories deduced from thermochronology, as well as stratigraphic studies of synorogenic deposits. In addition, the complex structural evolution of the St Elias region is broadly consistent with the predicted strain field evolution. **Citation:** Koons, P. O., B. P. Hooks, T. Pavlis, P. Upton, and A. D. Barker (2010), Three-dimensional mechanics of Yakutat convergence in the southern Alaskan plate corner, *Tectonics*, *29*, TC4008, doi:10.1029/2009TC002463.

1. Introduction

[2] In this paper we consider the geodynamics of the southern Alaskan margin as an orogenic system controlled predominantly by the collisional interaction of the Yakutat microplate with the northeast Pacific subduction-transform corner (Figure 1). We frame the entire plate corner within a single coherent three-dimensional thermal-mechanical model that permits examination of kinematics and dynamics at large scales (macroscale), as well as at the scales relevant to geological field observations (mesoscale). This mechanical framework allows the testing of the influence of boundary, surface, and thermally dependent rheological characteristics on the evolution of plate corner kinematics in the early stages of convergence.

[3] The collision can be considered as a distinct tectonic event along a long-lived plate corner where Pacific lithosphere moving parallel to the North American margin along the dextral Queen Charlotte/Fairweather transform system encounters the eastern syntaxis of the Aleutian trench megathrust (Figure 1). During subduction of normal oceanic lithosphere, this type of corner is stable and could persist for long periods with little complications beyond variations in sediment flux to the trench as sedimentary cover derived from the continent is carried laterally into the trench. In the southern Alaska orogen, however, subduction of normal oceanic lithosphere was disturbed when a slice of the North America margin, the Yakutat terrane, was plucked from the transform margin and carried northward into the trench where it flattens the subduction angle [*Plafker and Berg*, 1994; *Pavlis et al.*, 2004]. The thickened crust resting on the shallow-dipping mantle of this terrane together with its thick sedimentary cover is the principal driver for the Late Miocene to present orogenesis of southern Alaska, and thus, following *Pavlis et al.* [2004], we consider the geodynamics of the entire southern Alaskan orogen in the context of this collision.

[4] The margin of Alaska south of the Denali fault system has been the end point of terrane accretion since the Cretaceous [*Plafker and Berg*, 1994; *Eberhart-Phillips et al.*, 2006]. The assembly of the margin through the amalgamation of exotic terranes is consistent with the dominant tectonics of the Cordillera, of which the Southern Alaska orogen is the northern extent. As such, the study of the geodynamics of the Yakutat collision provides useful insight into the evolution the Southern Alaska orogen that

[1]Department of Earth Sciences/Climate Change Institute, University of Maine, Orono, Maine, USA.
[2]Department of Geological Science, University of Texas at El Paso, El Paso, Texas, USA.
[3]GNS Science, Dunedin Research Centre, Dunedin, New Zealand.
[4]Department of Earth and Space Sciences, University of Washington, Seattle, Washington, USA.

0278-7407/10/2009TC002463

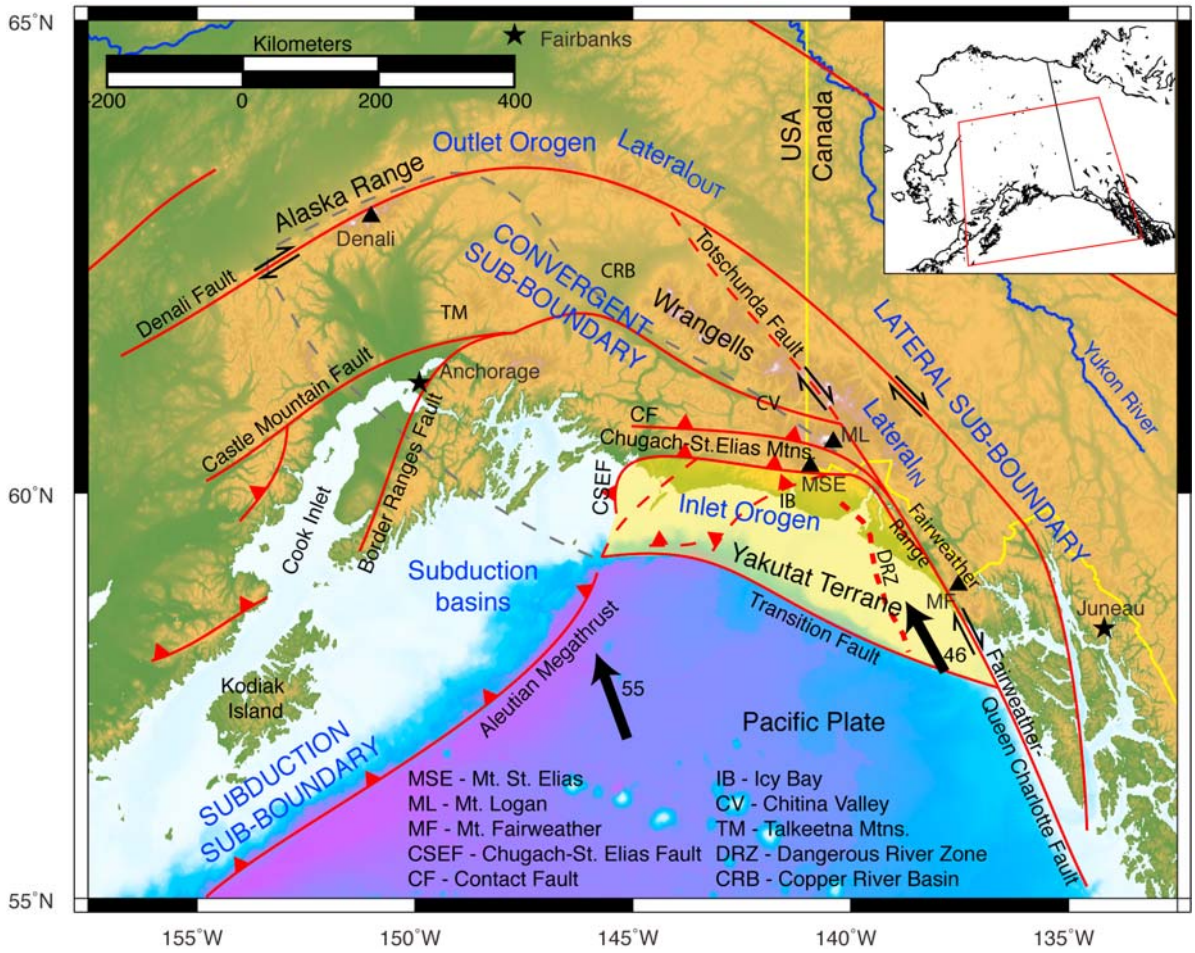

Figure 1. Map of southeastern Alaska showing the natural geometry of the study area plate corner, basic geology, and plate vector for the Pacific plate [*DeMets et al.*, 1994]. Shaded dashed outline indicates the extent of the Yakutat terrane in the subsurface based upon the seismic imaging completed by *Eberhart-Phillips et al.* [2006]. Major geologic features after *Plafker et al.* [1994a, 1994b]. Note the locations of Fairbanks, Anchorage, Denali, Mt. Logan, Mt. St. Elias, Mt. Fairweather, and the Alaskan coastline are used for spatial reference on Figures 2–9.

can be applied to the assembly of portions of the rest of the Cordilleran [*Pavlis et al.*, 2004].

2. Geodynamics of Southern Alaska

2.1. Present-day Morphology and Neotectonics

[5] At the scale of the entire plate boundary the orogenic system can be divided into five distinct elements (see Figure 1):

[6] 1. In southeastern Alaska, a narrow orogenic highland, the Fairweather Range, has developed along the dextral transpressive boundary between the Yakutat microplate and North America. High topography is restricted to the segment along the microplate boundary, and to the south there is little topographic expression of the Queen Charlotte transform system. This topographic variation has typically been attributed to an ~15° left-bend in the transform boundary (e.g., *Plafker et al.*, 1994a), but we note here that this topographic expression may be a natural consequence of the collision. In our models, we refer to this segment of the orogen as the Lateral subboundary.

[7] 2. Near the northernmost clear expression of dextral strike slip, both in surface geology and GPS, orogenic topography rises abruptly to form most of the high terrain in the orogen in what is geographically referred to as the Chugach-St. Elias Mountains and Wrangell Mountains. This region comprises the nexus of a series of complex interactions between the Lateral subboundary and the main orogen, and appears as a fundamental geodynamic feature in our modeling. We will refer to this nexus as the Lateral-Inlet subboundary.

[8] 3. To the west of the Lateral-Inlet surface geologic trends are generally subparallel to a major topographic highland that continues westward around the oroclinal bend of Alaska and decreases in elevation to the southwest, dropping below sea level to the southwest of Kodiak Island.

From Kodiak Island to approximately the longitude of Anchorage, this fore-arc highland may be more closely related to general subduction zone processes [e.g., *Pavlis and Bruhn*, 1983]. This part of the highland is underlain by subducting Yakutat microplate and merges with actively deforming fold-thrust systems of the collisional system. Within this actively deforming zone is an important geologic complication with a right-angle bend of the Yakutat terrane suture (Figure 1), which appears to reflect indentation of the margin by the colliding block [e.g., *Chapman et al.*, 2008]. In this paper, we refer to this fore-arc highland as the Inlet orogen.

[9] 4. To the north of the Inlet orogen is a distinctive lowland. West of Anchorage, this lowland consists of a deep sedimentary basin [*Bruhn and Haeussler*, 2006] but becomes geologically more complex toward the east. Specifically, a topographic highland, the Talkeetna Mountains, separates the Cook Inlet basin from a second basin, the Copper River basin, which also continues eastward as a deformed basin partially coincident with a narrow topographic low occupied by the Chitina River. Interestingly, the topographic lowland of the Copper River basin lies just inboard of the topographically lowest portion of the fore-arc highland. In this paper we refer to this general topographic lowland as the Subduction basins segment of the orogen.

[10] 5. Finally we note that to the north of the subduction basins segment is a second topographic highland that trends northwestward from the Lateral-Inlet forming a composite highland comprised of the Alaska Range and Wrangell Mountains. We refer to this northern highland as a composite feature because different segments of the highland are topographically and geologically distinct. The highland near to the Lateral-Inlet comprises the Wrangell Mountains, which are in part a bedrock high. However, the highest peaks in this location are large volcanic edifices of the Wrangell volcanic field that sit atop the bedrock high. This volcanic assemblage may be a short volcanic arc segment related to a small slab beneath the area [e.g., *Fuis et al.*, 2008] or more likely a volcanic assemblage constructed as a slab edge effect at the edge of the subducting Yakutat microplate [*Preece and Hart*, 2004]. The remainder of the high, including the highest peak in North America, Denali or Mt. McKinley, represents a constructed topographic highland developed through transpression along the dextral Denali fault system [e.g., *Nokleberg et al.*, 1994; *Miller et al.*, 2002]. The main uplift of this northern highland correlates closely in age to the collision of the Yakutat microplate [e.g., *Fitzgerald et al.*, 1995], implying a close connection between the two orogenic events. We consider this connection here, and refer to this northern highland as the Outlet orogen within the system and the $\text{Lateral}_{\text{Out}}$ subboundary connects the east side of Outlet orogen to the Lateral-Inlet.

2.2. Geologic History of the Orogen and Application of the Tectonic Model

[11] The southern Alaskan orogen (Figure 1) has been developing over more than 200 m.y. of earth history through a Mesozoic history of collisional accretion and dispersal of crustal fragments to a Cenozoic history that developed into the present north Pacific "elbow" containing a subduction to transform transition in southern Alaska (e.g., see *Plafker et al.*, 1994a). At ~30 Ma, the structural reorganization of the Aleutian subduction zone culminates in a eastward jump in the oblique transform boundary between North America and the Pacific plate, forming the proto-Yakutat terrane from the Cretaceous accretionary prism east of the Dangerous River Zone (DRZ; Figure 1) and near-trench Paleogene mafic intrusive basement rocks to the west of the DRZ [*Bruns*, 1983; *Plafker et al.*, 1994a; *Chapman et al.*, 2008]. This newly formed terrane was subsequently carried from its origin in the vicinity of British Columbia northward along the transform margin until it ultimately collided with North America within the present subduction-transform transition [*Plafker et al.*, 1994a; *Bruns*, 1983; *Perry et al.*, 2009]. During this northward translation the basement complex was buried by a thick (~7–10 km) Paleogene marine to fluvial sedimentary sequence (Poul Creek Formation) that is capped by glaciomarine synorogenic Yakutaga Formation deposited in response to Miocene orogenesis of the St. Elias Range [<6.5 Ma to present; *Plafker*, 1987; *Eyles et al.*, 1991; *Lagoe et al.*, 1993; *Zellers*, 1995; *Meigs et al.*, 2008]. The precise timing of the arrival of thickened crust of the Yakutat terrane and accompanied initiation of collisional tectonics is not well constrained, nor is the development of the present flat-slab subduction mode. Nonetheless, a few general constraints are sufficient for our analysis here.

[12] First, passive seismic studies [*Ferris et al.*, 2003; *Bauer et al.*, 2008] and offshore seismic studies [*Christeson et al.*, 2009; *Worthington et al.*, 2009] indicate that the Yakutat terrane basement is predominantly a thickened (>25 km) oceanic crustal section that presumably represents a subducted oceanic plateau. This thickened crust is now being subducted beneath the Alaska Range [*Ferris et al.*, 2003], and the leading edge of this thickened crust has been carried ~650 km from the present deformation front of the St. Elias orogen. Aside from small amounts of relative motion along the Transition fault (e.g., *Gulick et al.*, 2008; Figure 1) the Yakutat terrane is essentially carried with the Pacific plate (e.g., *Plafker et al.*, 1994a), which has converged with southern Alaska at 50–60 mm/yr since late Miocene time [e.g., *Engebretson et al.*, 1984]. Thus, the arrival of thickened crust and presumably development of the present flat slab began in the late Miocene, approximately 11–13 Ma. We assume that the present flat slab subduction mode developed sometime after that time interval.

[13] Second, this conclusion is supported by thermochronology studies [e.g., *O'Sullivan and Currie*, 1996; *Berger et al.*, 2008; *Meigs et al.*, 2008; *Enkelmann et al.*, 2008, 2009] and stratigraphic studies in the orogen [e.g., *Plafker et al.*, 1994a; *Zellers*, 1995] that indicate the initial uplift and associated exhumation of the North American backstop to the St. Elias orogen (Inlet Orogen of this paper) occurred in Late Miocene time (~10–15 Ma).

[14] Together these relationships suggest that the development of the present-day orogenic topography of southern Alaska is essentially a late Miocene to recent system. As such, we attempt to model the system in the context of flat

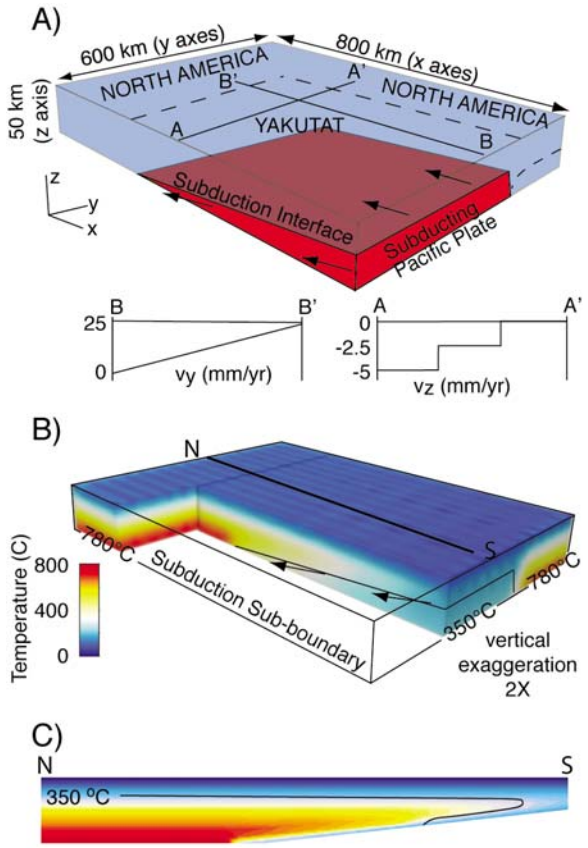

Figure 2. (a) Geodynamic model geometry and boundary conditions and (b) resultant thermal block model used to define mechanical models. (c) North–south cross section (location shown on Figure 2b) of the resultant thermal model used to define the mechanical model. The 350°C contour is indicated, approximating the transition between low temperature, pressure-dependent rheologies and temperature-dependent rheology. The surface temperature is fixed at 0°C, and the base of the model shown in Figure 2b is fixed at 780°C.

slab subduction in the modern geometry relevant to post ~5 Ma kinematics. Additionally 5 Ma is also an important time in the orogen because it was at that time the present plate motion mode was established. That is, 5 Ma was a well-known change in Pacific plate motion that produced an ~20° change in Pacific-North American motion, establishing the present transpressional mode of Queen Charlottes-Fairweather transform system [e.g., *Smith et al.*, 2003].

3. Terminology

[15] For the sake of brevity "uplift" is used to denote upwards-vertical material velocity, and "subsidence" denotes downward vertical velocity. We examine the orogen-scale strain patterns as well as the local-regional pattern of accommodation of orogen-scale strain at a scale relevant to regional structural geological studies and use macroscale to indicate plate corner wide patterns. At the macroscale, we divide the plate corner boundary into Convergent, Lateral, and Subduction subboundaries depending upon the far field relative plate kinematics (Figure 1). As discussed in sections 5 and 6, we further divide the subboundaries into kinematic elements defined in terms of the inlet and outlet flux boundaries. While recognizing that a continuum exists among these discrete components, we use these descriptive terms to investigate controlling influences in each subboundary and then look at the transitions among subboundaries. Mesoscale is used in the meteorological sense to denote patterns at the scale of meters to hundreds of kilometers of relevance to field and laboratory observations. Italicized terms refer to *Model* features and are employed to communicate the relationship of model to natural features (e.g., *Denali*, *St Elias*, *Fairweather*).

4. Numerical Modeling

[16] Three-dimensional thermal-mechanical numerical models were constructed to study orogen-scale macroscale and 100 km scale mesoscale kinematics and dynamics of the evolution of the Southern Alaska orogen. This model framework allows the testing of the influence of boundary, surface, and thermally dependent rheological characteristics on the evolution of plate corner kinematics during convergence. Our model geometry encompasses an area of dimensions 800 km (north–south = x) by 600 km (east–west = y) with a thickness of 50 km (= z) (Figure 2a). Grid spacing is 20 km horizontal and 5 km vertical. The geometry consists of a simple two-block representation of the large-scale tectonics of southern Alaska (Figures 1 and 2a). A wedge-shaped *Pacific block*, located in the southwestern corner of the model, is separated from the remainder of the model, the *North American block* inclusive of the *Yakutat terrrane*, by a frictional interface representing the Alaskan megathrust. All model boundaries are given fixed velocity conditions, except the surface, which is free to deform. Numerical solutions employed software (*Itasca Consulting Group, Inc.*, 1997; Fast Lagrangian Active Continuum; FLAC^{3D}) that approximates the stress and motion equations in the mechanical behavior of materials undergoing deformation at large strains [e.g., *Koons et al.*, 2002; *Upton et al.*, 2003]. FLAC^{3D} uses an explicit time-marching solution where each polyhedral element of the model responds according to a prescribed linear and/or nonlinear constitutive law in response to applied forces or kinematic boundary conditions [*Cundall and Board*, 1988].

[17] Our modeling strategy proceeds as follows:

[18] 1. Construction of a three-dimensional steady state thermal model for the plate boundary through solution of the nonlinear conduction:advection equation for the subduction geometry and kinematics modeled after the Pacific:North American plate boundary.

[19] 2. Use this three-dimensional thermal model to provide spatially varying temperature field to calculate rheological model (see section 4.1).

[20] 3. Produce a standard reference model to examine evolution of plate boundary deformation as a function of far-field relative plate velocities and our initial, thermally dependent rheology.

Table 1. Variables Used for Numerical Models

Variable		Value	
Density	ρ	2700	Kgm^{-3}
Bulk modulus	K	10^5	MPa
Shear modulus	G	3×10^4	MPa
Mohr-Coulomb Model			
Angle of friction	ϕ	35	degrees
Cohesion	S	100	MPa
Strain-Weakening Model			
Strain threshold	ε	0.03	
Angle of friction	ϕ_o	15	degrees
Cohesion	S_o	1	MPa
T-Dependent Flow Laws			
Gas Constant	R	8.31	$JK^{-1}mol^{-1}$
Strain rate	$\dot{\varepsilon}$	10^{-14}	s^{-1}
Wet Quartzite			
Activation energy	Q	134	$kJmol^{-1}$
Stress exponent	N_Q	2.60	
Material constant	A_Q	158	$MPas^{-1}$
Diabase			
Activation energy	E_D	260	$kJmol^{-1}$
Stress exponent	N_D	3.40	
Material constant	A_D	2×10^{-4}	$MPas^{-1}$
Thermal Model			
Specific heat	C_p	1000	$kJkg^{-1}K^{-1}$
Conductivity	κ	2.6	$Wm^{-1}K^{-1}$
Volumetric source	$A_{(x,y,z)}$	0.37	μWm^{-3}

[21] 4. Perturb the standard model by allowing strain-related rheological variation.

[22] 5. Apply erosion schema modeled after Alaskan glaciation to the rheologically evolved model.

[23] Here we wish to focus on the mechanical and structural evolution of the plate corner, so we present model times in the early stages of convergence while the essential mechanical characteristics are becoming established and until the deformation patterns stabilize. We present thermal results of numerical experiments and their geochronological implications for longer run times elsewhere [e.g., *Berger et al.*, 2008a].

[24] The three-dimensional kinematic boundary conditions of the model are based upon the relative motion of the Pacific:North American plate pair [Figure 2a; *DeMets et al.*, 1994]. The obliquity of the convergence is simulated within the model by applying a slight rotation of the basal boundary velocity vectors with convergence (Figure 2a inset cross section N-S (A-A′)). Additionally, the change from subduction of oceanic lithosphere to the more buoyant Yakutat terrane is simulated by changing the basal vertical velocity (= negative) across the model (Figure 2a inset cross section E–W).

4.1. Rheological Models

[25] The initial standard models consist of pressure-dependent *Yakutat* upper crust overlying a thermally activated lower crust, resting on an elastic *Pacific* dipping slab. The transition between the two crustal rheological models is defined dynamically as a function of local, transient temperature and strain rates in a manner constrained by experimental analysis [e.g., *Brace and Kohlstedt*, 1980; *Kohlstedt et al.*, 1995; *Mackwell et al.*, 1998; *Wijns et al.*, 2005]. We present a progression of rheological models commencing with a standard Mohr-Coulomb upper crust and plastic yield criterion lower crust based upon published power flow laws of the form $\dot{\varepsilon} = A\sigma^n e^{(-Q/RT)}$ (in which A is a preexponential factor, σ = differential stress (MPa), n = power law exponent, Q = activation energy, R = gas constant, T = temperature (K); see Table 1). We also investigate the effects of strain dependence on the upper crustal rheology. Surface boundary conditions are varied from passive deformation to active material erosion. Material properties for the constitutive models are provided in Table 1. Additionally, we test and discuss the sensitivity of the model results to variations in the rheological and surface boundary conditions.

4.2. Thermal-Rheological Model

[26] The strong dependence of crustal rheology on local temperature makes it imperative that the thermal behavior of the deforming region be fully characterized to a level of resolution compatible with the mechanical solutions. Consequently, we solve the three-dimensional transient conductive-advective Fourier equation, $\frac{\partial T}{\partial t} = \kappa\nabla^2 T + \frac{}{v}\nabla T + A_{(x,y,z)}$, over the same domain as the mechanical solution at the same discretization (κ = thermal diffusivity, m^2s^{-1}; $\vec{v}$ = kinematic velocity field, ms^{-1}; $A_{(x,y,z)}$ = radiogenic source, μWm^{-3}; see Table 1).

[27] In all experiments, surface temperature is maintained at 0°C [*Péwé*, 1975], as the region of interest is covered in glaciers, permanent snowfields, and local permafrost. A fixed temperature defines the base of the thermal model over the nonsubducting region of 780°C and an advective thermal gradient along the upper surface of the subducting Pacific plate [*Plafker et al.*, 1994a; *Pavlis et al.*, 2004; *Berger et al.*, 2008a]. The entire model domain is given an isotropic crustal thermal conductivity of 2.5 $Wm^{-1}K^{-1}$ and radiogenic heat production is uniform at 0.37 μWm^{-3}. The northern and eastern edges of the problem domain are conditioned as no-flux boundaries, while the southern and western edges are conditioned by the advective flux of the *Pacific plate* as discussed in section 5.1 (Figures 2b and 2c). The initial thermal solution is then used to assign constitutive rheologies for the mechanical model producing the frictional to viscous transition at ~350°C, consistent with the approximate temperature of the onset of crystal plasticity in quartz (Figure 2c) [e.g., *Hirth and Tullis*, 1992].

4.3. Strain-Dependent Rheological Model

[28] In the standard Mohr-Coulomb models we have employed an associated form of plasticity with post-yield stress levels maintained at the same as those at yield, however, natural materials typically exhibit rheological strain-dependence of strain-softening and/or strain-hardening behavior [*Vermeer and de Borst*, 1984]. Softening behavior generally leads to strain localization [*Hobbs et al.*,

1990; *Montési and Zuber*, 2002] and the formation of a pattern of low strain, nearly intact rock separated by high strain zones. To examine the consequences of localization on the strain patterns identified so far, we have used the same geometry and boundary conditions as the standard models but have employed a non-associated constitutive rheology for the upper brittle-frictional model crust. This strain-softening model assumes a form of initially intact cohesion (C) and friction angle (ϕ) (C = 100 MPa; ϕ = 35°) that weakens after 3% strain to lie within the typical range of fault rocks (C = 1 MPa; ϕ = 15°) [*Buck and Poliakov*, 1998].

4.4. Erosional Conditions

[29] The influence that surface processes have on the mechanical evolution of an active orogen is investigated by implementing simple erosional boundary conditions acting on the model surface. This erosion model removes mass from the model surface to maintain a constant elevation over the entire region of the Inlet orogen (160 km × 125 km). This is based on the assumption that glaciers and processes acting adjacent to glaciers (e.g., mass wasting) are capable of maintaining an approximately steady state elevation during orogenesis. This model region approximates the area in the St Elias region that contains the Malaspina and Bering glaciers where both the rate of uplift and the exhumation rate are poorly constrained, but some estimates imply that they are approximately of the same order of magnitude [*Hallet et al.*, 1996; *Meigs and Sauber*, 2000; *Berger et al.*, 2008b].

5. Model Results: Macroscale Kinematics

5.1. Thermal and Rheological Evolution

[30] Within active zones of deformation, the vertical component of the velocity field imposes severe control on the thermal and hence rheological state of an orogen (e.g., *Koons*, 1987; *Koons et al.*, 2002; *Hacker et al.*, 2003). The velocity field within this model corner generated by convergence of the 15 km thick model *Yakutat* material along a gently subducting *Pacific plate* characteristically contains paired material trajectories where incoming flow separates into a downward slab-dominated trajectory and an upward surface-dominated trajectory. Bifurcation of incoming lithosphere into upward and downward trajectories produces a pair of advective thermal anomalies that impart a distinctive rheological character to the models discussed below. Upward material trajectories, influenced in part by orographic precipitation concentration, can form a tectonic aneurysm parallel to the plate boundary [e.g., *Koons et al.*, 2002] and are examined within the context of coupled erosion and mechanics (see section 5.6).

[31] The downward trajectories associated with the subducting slab refrigerate the lower crust and produce a frictional sliver above the slab/crust interface that extends beneath the layer of ductile crust in the overlying plate (Figure 2c). This frictional sliver persists to depths well below the frictional-ductile transition that exists in the absence of advection and has long been recognized in subduction zones from seismicity distribution [e.g., *Abers et al.*, 2006; *Eberhart-Philips et al.*, 2006] Here we employ the thermal/mechanical model that incorporates these advection anomalies to examine the geodynamic implications of the frictional sliver within the context of the deforming plate corner. The main characteristics of the standard thermal model that we use as the basis of all mechanical modeling may be summarized as

- Thermal gradients across the incoming *Pacific/Yakutat block* are reduced relative to those in the *North American block* to the north and east due to advective cooling from the incoming cooler *Pacific/Yakutat block* (Figures 2b and 2c)
- Advective cooling related to the incoming *Pacific/Yakutat block* produces an inverted thermal gradient above the slab surface, leading to the formation of a frictional sliver extending down along the surface of the slab.
- The existence of this sliver is a robust function of advection, but the distance that the frictional sliver extends downdip is sensitive to the local Peclet number and therefore the choice of model material parameters. This frictional sliver is the numerical equivalent to the lower extent of the natural megathrust and, as discussed below, is a critical component of corner mechanics.
- Temperatures over the mantle wedge to the north range from 780°C at 50 km to 350°C at ~10 km, producing a slightly elevated ductile to frictional transition within the upper plate compatible with a subduction history prior to the arrival of the Yakutat block [*Plafker et al.*, 1994a].

[32] High thermal inertia of earth materials ensures that this pair of advective strength anomalies is spatially very stable and localizes contractional strain for the duration of the convergent event. Sensitivity analysis indicates that variations in the initial kinematics (i.e., changes to the local Peclet number) would cause changes to the extent and/or magnitude of the thermal advective signature, but not to the main characteristics described above.

5.2. Model Corner Deformation: Convergent Subboundary

[33] The Convergent subboundary initially forms as a relatively narrow (~50 km wide) two-sided orogen above the northernmost extent of the Pacific lithosphere as thoroughly predicted from analog, analytical, and two-dimensional numerical models [*Koons*, 1990; *Willett et al.*, 1993; *Whipple and Meade*, 2006] (Figures 3 and 4). As the plate boundary evolves with time and total convergence, deformation jumps ~ 500 km to the south and the Convergent subboundary is further separated into two, two-sided orogens, the Inlet orogen (toward the subduction zone with material entering the larger plate boundary) and Outlet orogen (on the continent side of the orogen, marking the tectonic exit of material). As defined, the Inlet and Outlet orogens identify kinematic elements that are general to convergent boundaries and not specific to southern Alaska.

[34] The location of the Inlet orogen is defined by the northward extent of the advective frictional sliver on the upper surface of the down-going slab. Strain becomes increasing concentrated into the Inlet orogen causing this deformation front to become the dominant location of strain

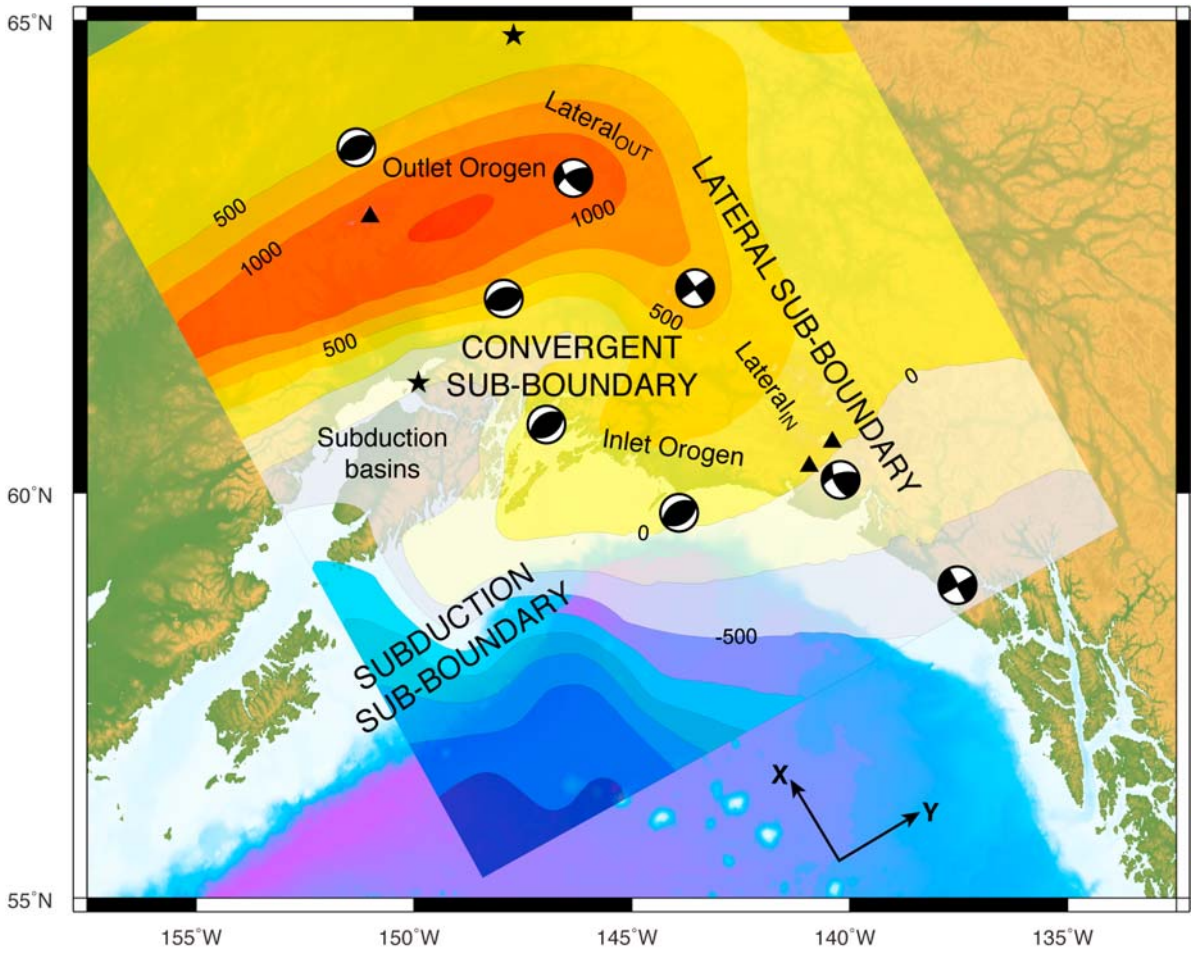

Figure 3. Diagrammatic sketch of the macroscale kinematic elements discussed in the text. Overlay onto basic study area map from Figure 1 shows the vertical displacement field (uplift; in meters) of the standard Mohr-Coulomb model results at 250 kyr.

release within the Convergent subboundary (Figures 3 and 4). Mechanical linkage between the Inlet and Outlet orogens is a function of rheological and erosional conditions as discussed below.

5.3. Lateral Subboundary

[35] For boundaries of sufficient length, oblique convergence along the lateral plate edge produces a narrow two-sided orogen with topographic steepness varying in part as a function of the material parameters, of the degree of obliquity in a manner predicted from the three-dimensional critical wedge approximation, and of the distribution and efficiency of surface erosional mechanisms [*Koons*, 1994; *Koons et al.*, 2003]. On the Inlet side (south) of the Convergent subboundary, the Lateral subboundary is manifest primarily by boundary-parallel strike slip faults equivalent to the Fairweather fault. Strain accommodation at the nexus of the Lateral and Convergent subboundaries is discussed in detail in section 6.

[36] Partitioning of convergent velocity into the Inlet orogen reduces convergent velocity (V_x) available for deformation in the Outlet orogen and results in the segmentation of the Lateral subboundary into a segment on the *Inlet* side of the plate boundary (=Lateral$_{In}$) and one between the Inlet and Outlet orogens (= Lateral$_{Out}$; Figure 3). Lateral$_{Out}$ subboundary transitions from predominantly strike slip near the Inlet orogen to dominantly contractional at the Outlet orogen (Figure 3).

[37] The segments of the Lateral subboundary are defined by the deformational fronts of the Inlet and Outlet orogens and result from the northward diminution in V_x as convergent strain is accommodated increasingly in the Inlet orogen. Consequently, lateral strain rates in the near surface along the Lateral$_{Out}$ segment are reduced by as much as an order of magnitude relative to Lateral$_{In}$ due to convergent deformation partitioning into the Inlet orogen (Figure 5). The amount of strain reduction along the Lateral$_{Out}$ segment is a partial function of the upper crustal rheological model as well as the distribution of erosion as discussed in Section 5.5. In all instances, the trend toward reduced $\dot{\varepsilon}_{XY}$ in the northern segments relative to south of the Convergent subboundary is a characteristic feature of the time-dependent growth of the plate corner.

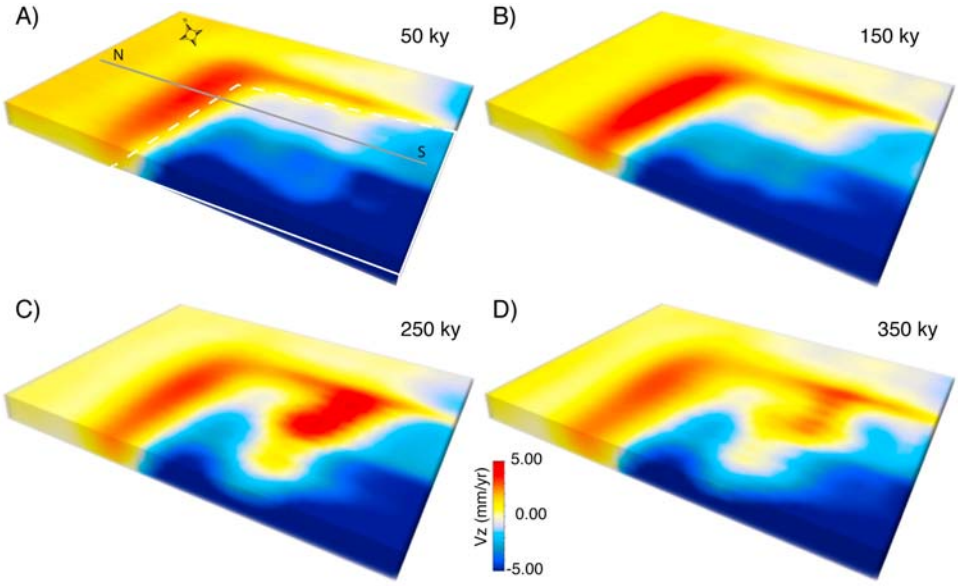

Figure 4. Vertical velocity (*Vz*) for the standard Mohr-Coulomb plate corner models illustrating the evolution of the plate boundary with time. The images are a time sequence of (a) 50 kyr, (b) 150 kyr, (c) 250 kyr, and (d) 350 kyr. Boundary and rheological conditions are as shown in Figure 2. The white line in Figure 4a outlines the limits of the Pacific plate, and the solid shaded line is the cross section line for Figures 5, 6, and 7.

5.4. Subduction Subboundary

[38] Subduction along the Aleutian trench forms the western limit of our model. The steeper dip of the subducting slab relative to the Yakutat accreting slab produces greater vertical subsidence, resulting in the formation of significant tectonic basins over the dipping subduction slab. Within the deforming regions, surface subsidence on any vertical column occurs when the mass dragged down by the subducting base exceeds the accretionary influx. This columnal mass balance is a function of the location and magnitude of contractional strain in addition to the relative values of the horizontal and vertical slab vectors. Consequently, the tectonic basins broaden to the west where the vertical velocity of the basal slab is greatest and narrow to the east where contractional strain is concentrated (Figures 4c and 4d). The formation and time-space evolution of these basins, and the implications to local stratigraphy are further explored elsewhere [*Kalbas et al.*, 2007; *Ridgway et al.*, 2007].

5.5. Influence of Strain-Softening Rheology

[39] The introduction of a material capable of brittle and frictional softening as a function of total strain damage produces generally similar kinematic elements to that of the standard Mohr-Coulomb models above with episodic shifts in the location of the deformation front (Figures 5 and 6). However, strain localization associated with softening leads to distinct strain concentrations and can strongly influence the timing of deformation, magnitude, and position of strain rate maxima. The progression of deformation fronts with increasing total convergence for a strain-softening material is clearly visible in cross sections at various times on the north-south profile through the **Inlet orogen** (Figures 5 and 6).

5.6. Mechanical Influence of Enhanced Erosion

[40] Application of a surface boundary condition to the strain-softening models that simulates constant, efficient erosion capable of maintaining steady state elevation within a model 160 km by 125 km stabilizes the strain pattern of the dual, coupled orogens (Figure 7). The imposed erosional steady state, on the southern side of the **Inlet orogen** results in three-dimensional strain patterns within the eroding zone similar to that described in fluvial-influenced orogens [e.g., *Koons et al.*, 2002; *Upton et al.*, 2009]. The erosional effect is dominated in this case by the influence of mass removal on vertical normal stress (σ_{ZZ}) as well as on the vertical shear stress components (σ_{XZ}, σ_{YZ}) as is typical of early stages of erosional influence [*Koons and Kirby*, 2007]. The nonlinear positive feedbacks of advective:erosional coupling that leads to the pattern of strain concentration characteristic of a tectonic aneurysm [*Zeitler et al.*, 2001; *Koons et al.*, 2002; *Koons and Kirby*, 2007] is in evidence in these models. The advective thinning of the high-strength upper crust in response to localized, concentrated erosion produces a distinctive thermal state present in the prototypical Himalayan, predominantly fluvial-driven aneurysm, and increasingly recognized in the thermochronology of southeast Alaska [e.g., *Zeitler et al.*, 2001; *Berger et al.*, 2008a; *Enkelmann et al.*, 2008; *McAleer et al.*, 2009]. In addition, aneurysm behavior also favors a stabilization of deformation front, producing vertical displacement maxima within the aneurysm and reducing the strain jumps produced for strain-softening material in the absence of tectonic:erosion cou-

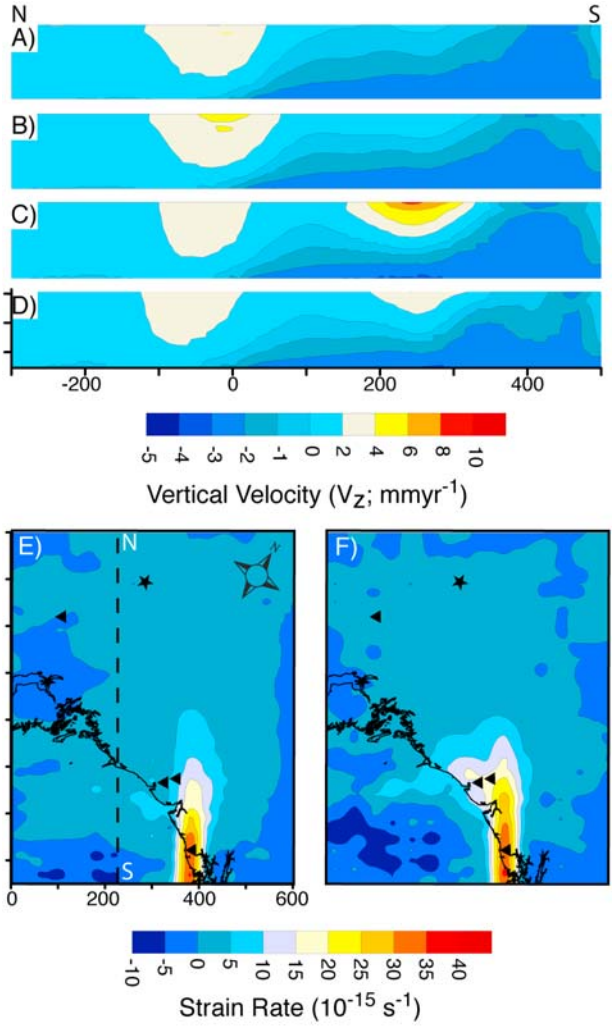

Figure 5. North–south cross sections showing vertical velocity (Vz; mm/yr) for the standard Mohr-Coulomb plate corner models illustrating evolution of the plate boundary. The images are a time sequence at (a) 50 kyr, (b) 150 kyr, (c) 250 kyr, and (d) 350 kyr. (e) Horizontal strain rate ($\dot{\varepsilon}_{XY}$; s^{-1}) at the surface (~1 km depth) in early stages of convergence (50 kyr) prior to significant partitioning of convergent velocity (V_X) into the inlet orogen. (f) $\dot{\varepsilon}_{XY}$ at the surface (~1 km depth) in later stages of convergence (250 ky) when convergent velocity (V_X) is partitioned in the Inlet orogen, reducing the amount of horizontal shear strain on the Lateral$_{out}$ segment of the Lateral subboundary.

pling (Figure 7). The thermochronological implications of this behavior are explored elsewhere [*Enkelmann et al.*, 2008].

6. Model Results: Mesoscale Kinematics

[41] The large-scale convergent, oblique, and strike slip deformation patterns produced during corner evolution are accommodated at the mesoscale (meters to hundreds of kilometers) by a characteristic pattern of strain knots at the joins between the various subboundaries. These knots are produced by spatial concentrations of shear strain in the horizontal plane ($\dot{\varepsilon}_{XY}$) and vertical shear strain rates along planes parallel to and normal to the Lateral subboundary ($\dot{\varepsilon}_{XZ}$, $\dot{\varepsilon}_{YZ}$). This "strain trinity" of maxima in the Cartesian strain rate components ($\dot{\varepsilon}_{XY}$, $\dot{\varepsilon}_{XZ}$, $\dot{\varepsilon}_{YZ}$) displays predictable temporal and spatial variations as the plate corner evolves (Figure 8). In the early stages of convergence prior to the spatial separation of the Inlet and Outlet orogens, shear strain along the Lateral subboundary extends directly into a

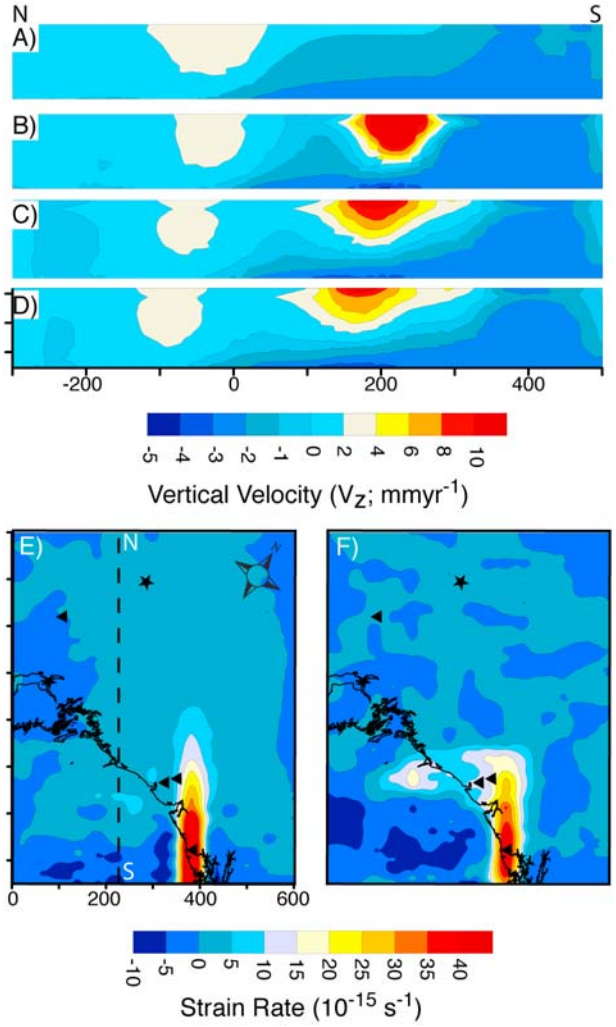

Figure 6. North–south cross sections showing vertical velocity (V_Z; mm/yr) for the strain-softening plate corner models illustrating evolution of the plate boundary. The images are a time sequence at (a) 50 ky, (b) 150 ky, (c) 250 ky, and (d) 350 ky. (e) $\dot{\varepsilon}_{XY}$ at the surface (~1 km depth) in early stages (50 ky) of convergence prior to significant partitioning of convergent velocity (V_X) into the inlet orogen. (f) $\dot{\varepsilon}_{XY}$ at the surface (~1 km depth) in later stages of convergence (250 ky) when convergent velocity (V_X) is partitioned in the Inlet orogen, reducing the amount of horizontal shear strain on the Lateral$_{out}$ segment of the Lateral subboundary.

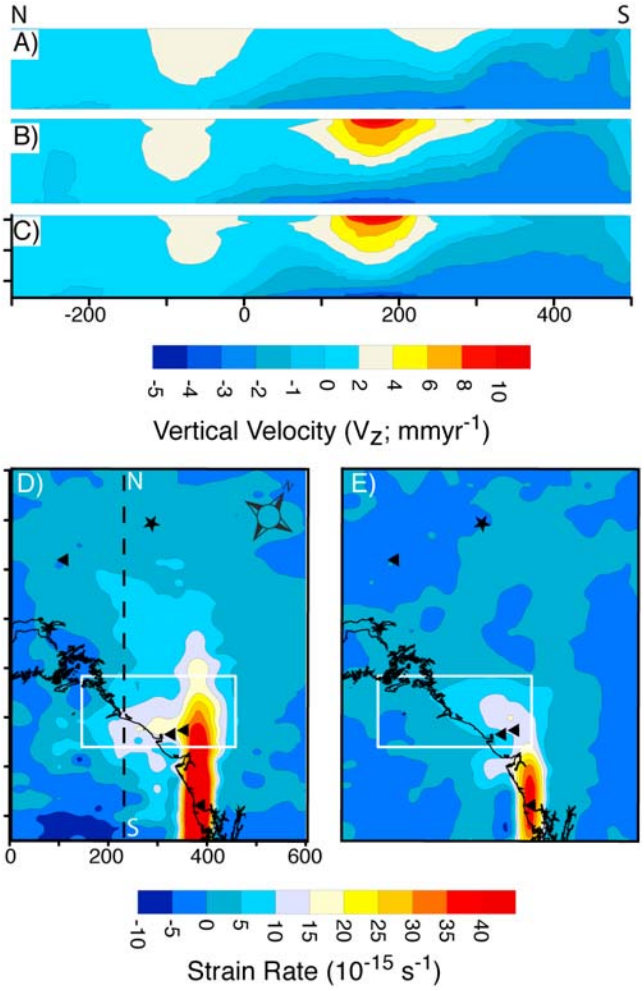

Figure 7. North–south cross sections showing vertical velocity (V_Z; mm/yr) for the erosional plate corner models illustrating evolution of the plate boundary. The images are a time sequence at (a) 50 ky, (b) 150 ky, and (c) 250 ky. (d) and (e) $\dot{\varepsilon}_{XY}$ for model with regional erosion at 50 and 250 ky, respectively. All map views are at shallow (~1 km) crustal depths. Boxes on Figures 7d and 7e indicate the area of regional erosion.

two-sided oblique orogen with oppositely dipping shear zones that bounds the corner of the orogen (Figures 8a, 8b, and 8c). During this stage, shear along the lateral boundary is dominant; thus, the strain rate term $\dot{\varepsilon}_{XY}$ dominates the kinematic field, whereas $\dot{\varepsilon}_{XZ}$ and $\dot{\varepsilon}_{YZ}$ remain relatively low within the upper crust (<5 km). At the corner, transition from predominantly strike-slip kinematics through oblique shortening to fully convergent strain is accommodated by oppositely dipping oblique structures that wrap smoothly along the Outlet orogen and more abruptly at the Inlet-Lateral join.

[42] As strain is increasingly shifted to the Inlet orogen, the strain trinity at the Inlet-Lateral join also shifts toward the Inlet, separating the single strain pattern into two strain knots, each exhibiting the characteristic strain trinity, and associated with the Lateral terminations of the Outlet orogen and the Inlet orogen. As mentioned above, this shift leads to a reduction in strain rate along $\text{Lateral}_{\text{Out}}$, the Lateral subboundary segment that lies between the Inlet and Outlet orogens, with a consequent reduction in the magnitude of the strain rates associated with the Outlet orogen strain trinity (Figures 8d, 8e, and 8f).

[43] As a consequence of the strain rate shift with maturation of the Inlet orogen, the structural history along the Inlet-Lateral subboundary intersection (= model *St. Elias*) displays a characteristic kinematic sequence of initially predominantly strike slip accommodating lateral shear in the early stages of plate corner evolution, overprinted by the mix of oblique structures of the strain trinity. If the crust is capable of strain softening, the Inlet strain knot accommodating the strain trinity becomes a region of focused deformation leading to regions of rapid uplift and high elevations of the present model St. Elias.

7. Numerical Model Sensitivity

7.1. Thermal/Rheological Model

[44] We have employed observations from seismic analysis compatible with ocean crust for at least part of the Yakutat terrane to develop the model geometry, boundary kinematics, and initial thermal state of the plate boundary [*Pavlis et al.*, 2004; *Abers et al.*, 2006; *Eberhart-Philips et al.*, 2006]. The general thermal state of the model, and consequently the rheological state, is influenced by the initial thermal state of the plate boundary. Additionally, zones of vertical material advection associated with the shallow subduction of the slab, with its associated cooling at depth further influence the thermal and mechanical state of the model. The initial thermal state may vary significantly depending on the degree of prior and current asthenospheric involvement as well as due to the earlier ridge interaction with the plate boundary [*Pavlis and Sisson*, 2003]. In a general sense, the higher the initial temperatures in the *North American plate,* the greater the separation of Inlet and Outlet orogens as the advective frictional sliver develops. The advection pattern, however, is a partial function of the convergence velocities and surface processes and is therefore not very sensitive to the initial state. Taken together, the general asymmetric shape of the thermal model is characteristic of convergence where collision is preceded by subduction, and this asymmetry produces an orogen with the geometry described here. Consequently, the thermal/rheological model is robust in its general characteristics although the magnitude of deformation will vary as a function of the model-specific boundary, initial state, and rheological conditions.

[45] Our choice of strain-softening model that allows cataclasite weakening of both brittle and frictional material properties [i.e., *Buck and Poliakov*, 1998], results in enhancement of each of the kinematic elements described above. Weakening influences the development of strain partitioning into areas of localization, suggestive of shear zones or faults while the remaining model remains relatively undeformed. As demonstrated by comparison of the models

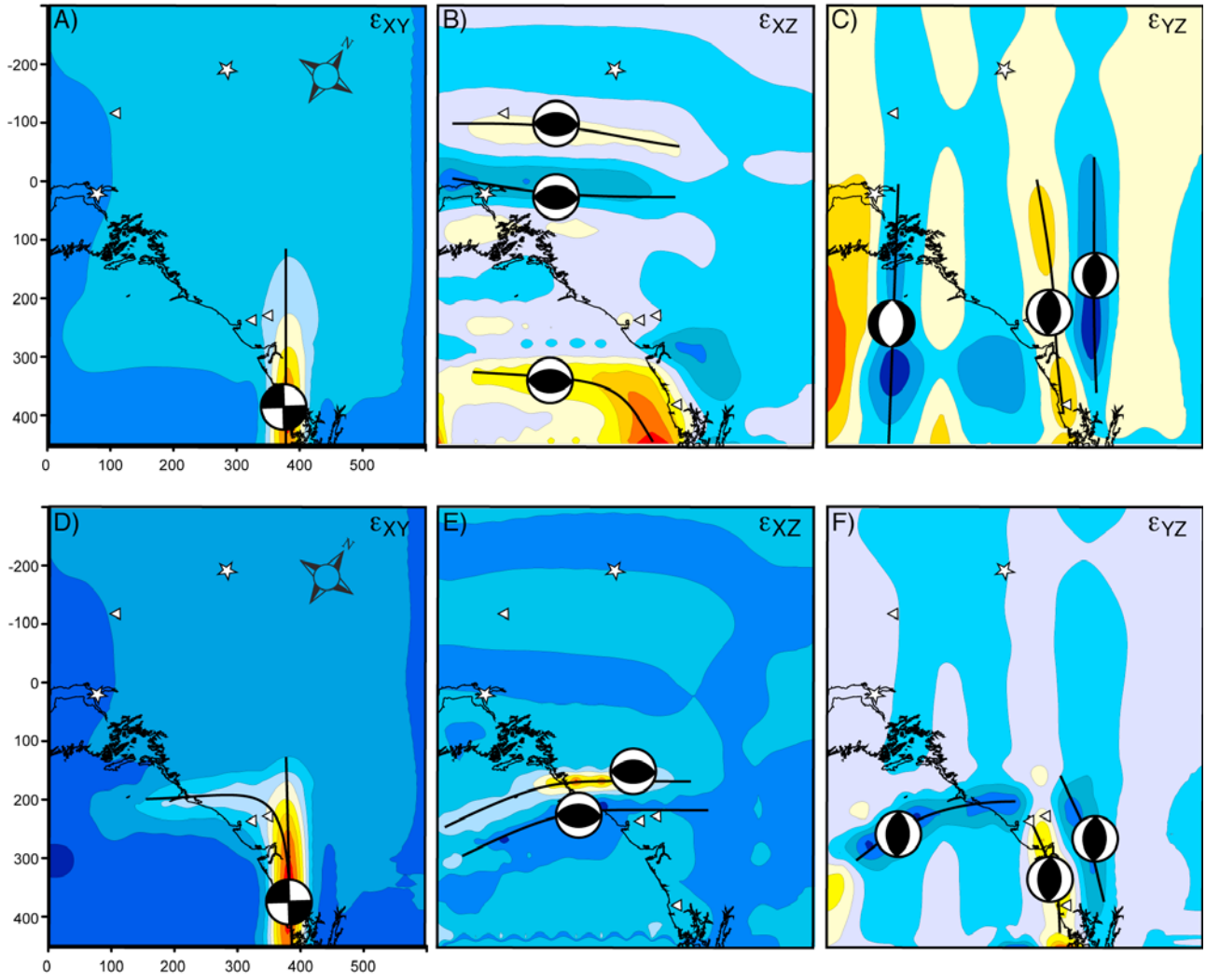

Figure 8. Mesoscale displacement architecture of the strain trinity from the strain-softening model at (a, b, c) 50 ky and (d, e, f) 350 ky. Plotted are filled contour patterns of $\dot{\varepsilon}_{XY}$, $\dot{\varepsilon}_{XZ}$, and $\dot{\varepsilon}_{YZ}$ along a surface at ~ 1 km below modern sea level. First motion symbols provide a qualitative indicator of strain orientation. In this strain-softening model, the concentration of the three strain components shifts to the south along the Lateral boundary with increasing convergence.

with and without strain softening, the general kinematic pattern of the deforming corner is not very sensitive to strain weakening; however, the amount and location of strain concentrations are sensitive to the choice of rheological model.

7.2. Model Limitations

[46] In order to concentrate on crustal and surface deformation, we have chosen to develop our models with the present trajectories of the Yakutat fragment resting on a subducting Pacific plate using seismic observations of shallower subduction beneath the Yakutat fragment than beneath the Aleutian arc [e.g., *Eberhart-Phillips et al.*, 2006]. This choice precludes an examination of the interaction of buoyancy and viscous forces within the full crust-lithosphere-asthenosphere system. This component of mantle influence is examined in detail elsewhere [e.g., *Billen and Hirth*, 2006]. Also precluded is a full dynamic model of the first impingement of the flattening slab beneath the orogen. Timing relationships and geometry for this poorly known transition to the modern geometry are derived from geochronological information.

[47] The advective perturbation of the crust and mantle thermal state by subduction, both shallow and steep, leads to abrupt three-dimensional geothermal gradients with consequent spatial complexity of mineralogical stabilities [e.g., *Hacker et al.*, 2003]. Our choice of rheological models in which effective viscosity is a partial function of compositional and thermal variables inadequately captures reaction-induced rheological variation. This reaction-induced rheological influence derives from changes in mineralogy, grain size, local pore pressure, buoyancy, and viscosity, with implications to surface kinematics and ultra high pressure

metamorphism that are currently under investigation [*Whipple and Meade*, 2006].

8. Summary of Mechanics: Controlling Variables and Teleconnections

[48] Dynamics and kinematics of all subboundaries within the evolving plate corner are linked through local rheology and the pattern of surface processes. The driving force for deformation on each of the subboundaries arises from shear coupling along the *Pacific:Yakutat* basal boundary. The instantaneous force balance can be perturbed by temporal variation in any of these components.

[49] In general, strengthening along the subduction interface related to advective cooling, metamorphic reaction, or strain hardening will result in transfer of strain to the Outlet orogen and an increase in strain rates within the Outlet orogen (model *Denali)* and the $\text{Lateral}_{\text{Out}}$ subboundaries. Similarly, reduction in strength along the subduction interface, plausibly arising from reaction weakening, pore pressure increases (and modeled above as strain softening; Figure 6) result in strain partitioning into the Inlet orogen and reduction in strain rates of the Outlet orogen and $\text{Lateral}_{\text{Out}}$ subboundaries.

[50] Plate corners are sensitive to variations in vigor and location of surface erosional activity with teleconnections exhibited at two distinct scales, Intraorogen and Interorogen. Focused erosion along the Inlet orogen concentrates strain into the actively eroding Inlet slope while reducing strain in the Outlet orogen and the associated $\text{Lateral}_{\text{Out}}$ subboundaries.

[51] Although the southern Alaskan orogen contains most of the highest peaks in North America and includes the highest coastal mountain range on Earth, surprisingly little attention has been directed at the origins of this orogenic system. North America's highest peak, Mt. McKinley/Denali, has long been recognized as a direct consequence of a restraining bend on the dextral Denali fault system [e.g., *Stout and Chase*, 1980], and the St. Elias Mountains have long been linked to collisional tectonics of the Yakutat terrane [e.g., *Plafker et al.*, 1978]. Nonetheless, researchers have only recently emphasized the close relationships among the various elements of the southern Alaskan orogen [*Fletcher and Freymueller*, 1999; *Haeussler et al.*, 2003; *Pavlis et al.,* 2004; *Bruhn et al.*, 2004; *Eberhart-Philips et al.*, 2006; *Redfield et al.*, 2007], although the concept is not new [e.g., *Plafker*, 1965; *von Huene and Scholl*, 1991; *Scholl et al.*, 1992]. The modeling discussed here drives home the importance of the close connection between different elements of the southern Alaskan orogen and makes specific predictions that are broadly consistent with known geologic histories in southern Alaska.

[52] Perhaps the simplest, first-order prediction of our geodynamic models is that during flat-slab convergence in an orogenic system like the southern Alaskan orogen, the orogenesis initiates with uplift along the oblique orogen with displacements transferred into the outlet orogen. With time, the system evolves and deformation steps toward the inlet orogen. In addition, the models predict that at the intersections of the oblique orogen with the inlet and outlet orogens, localized zones of high and rapidly changing strain rate are developed as material is transferred from the oblique into the convergent Inlet and Outlet orogens. In terms of the southern Alaskan orogen, the models therefore predict that the orogen should have initiated with oblique-convergence along what is now the Fairweather fault transferring deformation onto the continental margin to form the Alaska Range. With time, however, deformation should step toward the inlet orogen, concentrating deformation and uplift into what is now the Chugach-St. Elias Mountains. Unusual structural and exhumational histories are also predicted in the region where the oblique orogen intersects the Inlet and Outlet orogens. Two major lines of geologic evidence are consistent with this prediction:

[53] 1. *Thermochronologic Evidence:* A low-T thermochronologic database exists for much of southern Alaska, particularly the St. Elias orogen [*Berger et al.*, 2008a, 2008b; *Berger and Spotila*, 2008; *Enkelmann et al.*, 2008] and the Alaska Range [*Fitzgerald et al.*, 1995; *Haeussler et al.*, 2008; *Haeussler*, 2008]. These data provide significant constraints on the exhumation histories of both the Inlet (St. Elias) and Outlet (Alaska Range) orogens that are consistent with our modeling. The simplest evidence is a direct comparison of apatite fission track age versus elevation data for the two largest massifs in the two parts of the orogen: Denali in the Alaska Range [*Fitzgerald et al.*, 1995] and Mt. Logan in the St. Elias Range [*O'Sullivan and Currie*, 1996]. Both of these massifs show remarkably well preserved partial annealing zones at high elevations, consistent with very young uplift and exhumation, but the timing between the two massifs is distinctly different (Figure 9). On Denali, a single partial annealing zone is preserved indicating an onset of uplift and exhumation at ~5–7 Ma [*Fitzgerald et al.*, 1995] and ~6 Ma most likely from the data. In contrast, Mt. Logan preserves two partial annealing zones with an early exhumation in the late Miocene (~14 Ma), but the main exhumation is associated with the modern topography initiating at ~4 Ma [*O'Sullivan and Currie*, 1996]. The latter is particularly significant because it is ~2 m.y. younger than the initiation of uplift and exhumation recorded at Denali, a relationship consistent with the model predictions. Further evidence for this distinction in the timing of uplift and exhumation is provided by regional thermochronology data sets, although these data are more difficult to interpret because they contain a more complex signal related to variable sample elevations and variable sampling densities. Nonetheless, crude comparisons broadly support the concept that the main uplift and exhumation is now concentrated in the Inlet orogen (Chugach-St. Elias Mountains) but that uplift and exhumation is very young. Specifically, the St. Elias Mountains show extremely young U-Th-He apatite ages (<1 Ma) ages along the windward flank of the range where extreme glacial erosion rates predominate [*Fletcher and Freymueller*, 2003; *Berger et al.*, 2008a; *Berger and Spotila*, 2008], yet higher temperature thermochronometers (e.g., zircon fission tracks and zircon U-Th-He) were generally not reset from their detrital ages. This suggests that although extreme exhumation rates have characterized the Pleistocene, those rates could not have occurred as recently as the Pliocene (*Berger et al.*, 2008b).

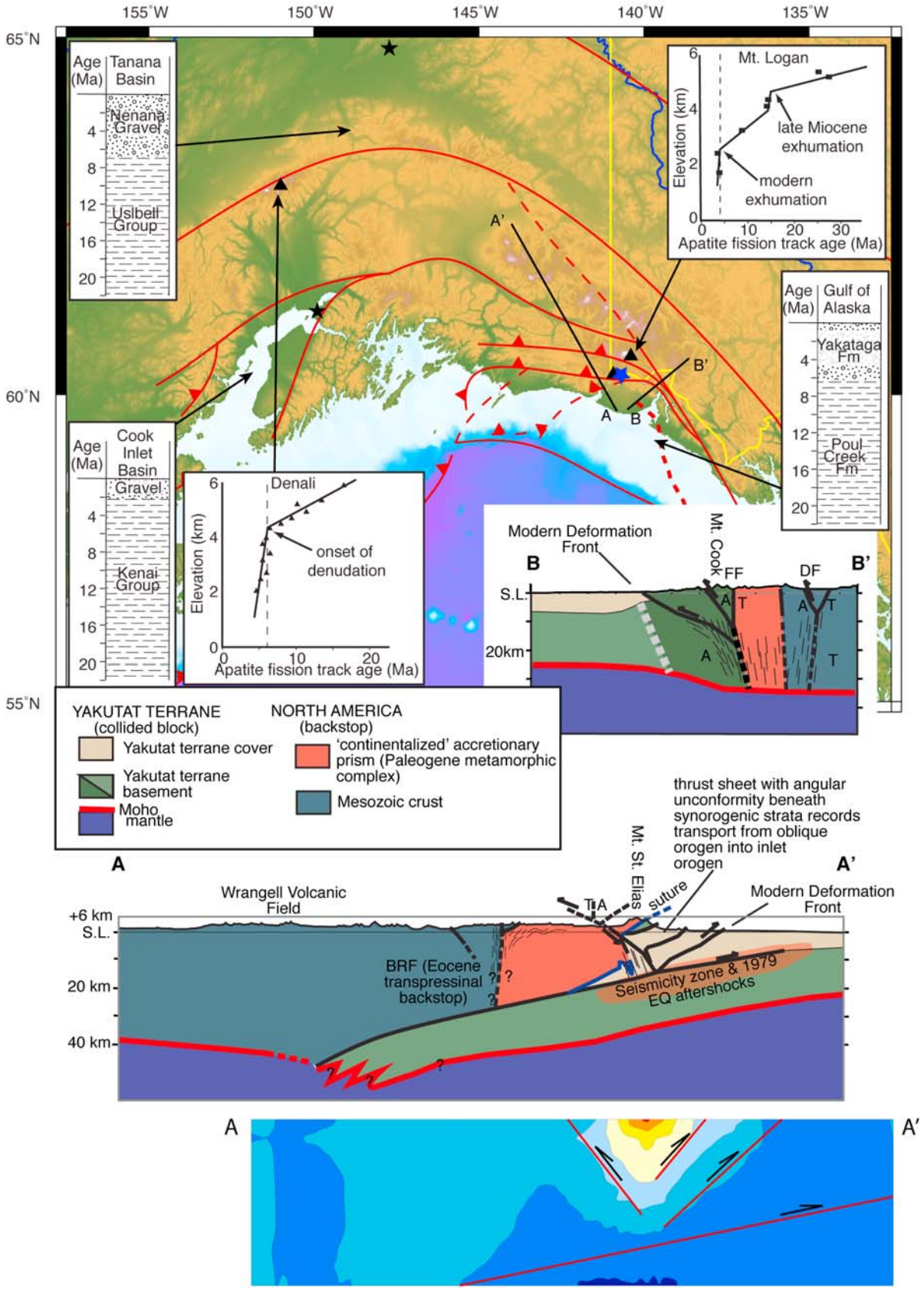
155°W
150°W
145°W
140°W
135°W
65°N
60°N
55°N
Age (Ma)
Tanana Basin
Nenana Gravel
Usibell Group
Mt. Logan
Elevation (km)
late Miocene exhumation
modern exhumation
Apatite fission track age (Ma)
A'
B'
A
B
Age (Ma)
Gulf of Alaska
Yakataga Fm
Poul Creek Fm
Age (Ma)
Cook Inlet Basin
Gravel
Kenai Group
Denali
onset of denudation
Elevation (km)
Apatite fission track age (Ma)
Modern Deformation Front
Mt. Cook
FF
DF
B
B'
S.L.
20km
A
T
YAKUTAT TERRANE
(collided block)
Yakutat terrane cover
Yakutat terrane basement
Moho
mantle
NORTH AMERICA
(backstop)
'continentalized' accretionary prism (Paleogene metamorphic complex)
Mesozoic crust
A
A'
thrust sheet with angular unconformity beneath synorogenic strata records transport from oblique orogen into inlet orogen
Mt. St. Elias
suture
Wrangell Volcanic Field
TiA
Modern Deformation Front
+6 km
S.L.
20 km
40 km
BRF (Eocene transpressinal backstop)
Seismicity zone & 1979 EQ aftershocks
A
A'

Figure 9

Although this exhumation is strongly linked to climatic changes of the Pleistocene [*Berger et al.*, 2008b], these data also indirectly imply that deformation rates also have accelerated during the Pleistocene within the St. Elias Mountains, a generalization broadly consistent with deformation stepping outboard, toward the Inlet orogen.

[54] 2. *Stratigraphic Evidence:* The sedimentary record from three large basin systems within the orogen provides an alternative record of the uplift history in the orogen: the Cook Inlet basin, the Tanana Basin, and the offshore Gulf of Alaska basin systems. The Tanana basin provides the most direct record of uplift related to the Alaska Range because it is isolated from surrounding parts of the orogen by the Alaska Range itself, and has distinctive geologic source terranes that contributed to the basin [*Ridgway et al.*, 2007]. *Ridgway et al.* [2007] provided a comprehensive picture of the evolution of this basin in the context of orogenesis in the Alaska Range and concluded that the Alaska Range was a developing highland by the time of deposition of the middle Miocene Suntana Formation (~15 Ma). Moreover, there is no doubt that the Alaska Range was a major orogenic source by the time of the transition from the deposition of the Grubstake Formation to the deposition of the Nenana Gravels, which is now well dated at 6.7 Ma [*Ridgway et al.*, 2007]. Indeed, this onset of coarse clastic sedimentation corresponds closely in age to the onset of rapid exhumation of the Denali massif indicated by *Fitzgerald et al.* [1995], and suggests initial orogenesis of the Alaska Range began in the middle Miocene, but exhumation accelerated at ~6.5–7 Ma [*Ridgway et al.*, 2007].

[55] In contrast, the sedimentary record in the Gulf of Alaska, on the trailing edge of the colliding Yakutat microplate, the onset of synorogenic sedimentation appears to be distinctly younger. The synorogenic deposits of the Gulf of Alaska basin are referred to as the Yakataga Formation and contain a complex depositional system with numerous synorogenic unconformities as well as facies variations related to the dominance of glaciomarine sedimentation of the unit. The exact age span of the unit has been a long-standing issue because of poor paleontological age constraints [e.g., *Plafker*, 1987], but recent work strongly suggests the unit is entirely latest Miocene to recent in age. At Yakataga Reef, for example, the base of the synorogenic section is exposed and well dated at between 5.6 and 5.0 Ma [*Eyles et al.*, 1991; *Lagoe et al.*, 1993]. Admittedly, it is possible that older synorogenic deposits may be present (up to 6.5 Ma), but this exposure is essentially at the deformation front of the orogen, and it seems unlikely to be disturbed by nondeposition on a local high. Similarly, *Lagoe and Zellers* [1996] used microfossils from offshore exploration wells and concluded that the Yakataga section was entirely Plio-Pleistocene, dated at ~5.6 Ma and younger. Moreover, they showed clear evidence of dramatic increases in sedimentation rates with time, indicating increasing uplift and exhumation in the adjacent St. Elias orogen (Inlet orogen).

[56] Together these stratigraphic observations support the predictions of the models, with orogenesis occurring earlier in the Alaska Range (Outlet orogen) than the St. Elias range (Inlet orogen). At a minimum, the onset of coarse clastic wedges shed from both ranges show a time lag of < 1 to ~2 m.y., analogous to the thermochronology data, but the *Ridgway et al.* [2007] suggestion of an even older initiation of uplift in the Alaska range (~15 Ma) suggests the possibility of an even greater time differential between onset of orogenesis in the Alaska Range versus the St. Elias Range.

[57] 3. *Structural Evidence:* The local structural history on the colliding block also provides evidence consistent with the models, particularly the prediction of complexities at the "nexus" where the oblique orogen interacts with the Inlet orogen. Even in the absence of the models it is qualitatively clear that the kinematics of this region should be complex as material on the colliding block is transferred along the oblique orogen segment before arrival at the nexus. The model provides further insight into this process; however, because at this nexus the strain trinity becomes large predicting complex, high-strain rates deformational shifts as crustal blocks are transferred into the nexus (Figure 9). Indeed, several complexities that are broadly consistent with this history are observed. First, this region contains the highest topography within the orogen, consistent with high-strain rates operating in this zone, despite other evidence for extreme erosion rates within this region [e.g., *Enkelmann et al.*, 2008]. Second, this area shows some of the most intense seismicity within this segment of the orogen and was the site of a large historic earthquake (1979 M 7.4 M_w) [*Estabrook et al.*, 1992] (see Figure 8) along a northwest dipping fault, a trend dramatically oblique to the local topographic trend. Third, geologic studies show complex fault overprints that vary with the stratigraphic level suggesting marked changes in stress states over time in this region [*Chapman et al.*, 2008]. Of particular note are differences in fold trends across a major angular unconformity between synorogenic strata and preorogenic strata in the Samovar Hills [e.g., *Bruhn et al.*, 2004; *Chapman et al.*, 2008] consistent with temporal rotational in strain fields in this region. Finally, individual thrust sheets in the Icy Bay region (Figure 1) show along-strike variations in development of an angular unconformity beneath the synorogenic Yakataga Formation and show evidence of complex out-of-sequence thrusting,

Figure 9. Synthesis of observed geology of the study area incorporating thermochronology, sedimentology, and structural geology. Age elevation plots from Denali [*Fitzgerald et al.*, 1995] and Mt. St. Elias [*O'Sullivan and Currie,* 1996] illustrate the dichotomy in timing of uplift between the two regions of the study area. Uplift is also tracked by the formation and infilling of basin in the Copper River, Gulf of Alaska, and Cook Inlet [e.g., *Kalbas et al.*, 2007; *Eyles et al.*, 1991; *Lagoe and Zellers,* 1996]. Similar patterns of deformation are observed within the geological cross sections A–A′ and B–B′ as those patterns of deformation that are predicted from the mechanical models. The blue star located just east of Mt. St. Elias shows the approximate location of the 1979 M 7.4 M_w earthquake [*Estabrook et al.*, 1992]. The model cross section covers the same area as A–A′ and has structural interpretations for comparison to the geological cross section.

observations broadly consistent with major temporal changes in strain rate components.

9. Conclusions

[58] The macroscale kinematic elements of Yakutat convergence along the southern Alaska plate boundary (Inlet, Outlet convergent orogens, segmented Lateral boundary, and Subduction basins) are characteristic of plate corner convergence and arise from thermal/rheological nonlinear interactions dominated by vertical material velocity. Subduction quenching due to advection of cooler material into the orogen produces a high-strength frictional sliver along the subduction interface that controls the position of the Inlet orogen. Increasing the differences between the Inlet and Outlet thermal regimes enhances separation of the Inlet and Outlet orogens. The greatest separation between the two orogens occurs with an initially elevated thermal regime beneath the Outlet orogen and severe advective cooling beneath the Inlet orogen.

[59] Mechanical coupling within the plate corner leads to teleconnections among all subboundaries. Consequently, temporal variation in rheological parameters or surface processes along any subboundary is reflected in potentially observable changes in strain rates along the other subboundaries. For example, strain weakening or enhanced erosion rates in the Inlet orogen lead to steady shifting of deformation toward the Inlet orogen with associated reduction in strain rates within the Outlet orogen and the $\text{Lateral}_{\text{Out}}$ segment of the Lateral subboundary. Consequently, we predict from the coupled mechanical models that climatic-induced erosional changes in the St Elias region of the Inlet orogen has altered the deformation pattern in the Denali region and along the eastern lateral bounding faults of the Fairweather and Denali fault systems. The present oceanic and atmospheric circulation patterns of the Gulf of Alaska enhance concentration of deformation along the Inlet orogen subboundary at the expense of the Outlet subboundary.

[60] A strain trinity of coincident $\dot{\varepsilon}_{XY}$, $\dot{\varepsilon}_{XZ}$, and $\dot{\varepsilon}_{YZ}$ maxima represents the characteristic mesoscale form of the transition from oblique lateral accretion to normal convergence at plate boundary internal corners. This strain trinity forms to accommodate the changing bounding velocities, links regional to orogen scale structures, and is expressed as opposite dipping shear zones. The strain rate knots at the intersection of convergent and lateral boundaries increase in separation with increased deformation, defining a lateral zone between these intersections of lower $\dot{\varepsilon}_{XY}$ relative to that on the Inlet side of the plate boundary.

[61] In all instances, the trend toward reduced $\dot{\varepsilon}_{XY}$ along the $\text{Lateral}_{\text{Out}}$ segment relative to that on the Inlet side of boundary is a characteristic feature of the time-dependent growth of the plate corner.

[62] Incorporation of strain-softening rheology enhances the separation of the coupled dual orogens while application of simple steady state erosional surface conditions over an area of dimensions similar to those of the Malaspina-Bering glaciers results in concentration of strain and stabilizes the growth of the orogen leading to the early stages of tectonic aneurysm development driven by glacial erosional processes.

[63] If, as we argue from our continuum modeling, the macroscale and mesoscale strain patterns that accompany Yakutat convergence in southern Alaska are characteristic of plate corner tectonics, then the deformation field described here can provide insight into the early stages of convergence along other plate corners, specifically the Eastern Syntaxis of the Himalaya where the early history of convergence has been obscured by subsequent events.

[64] **Acknowledgments.** Discussions with other STEEP participants, notably B. Hallet, P. Zeitler, E. Enkelmann, S. Gulick, and J. Spotila have significantly influenced our modeling. Julie Elliot kindly supplied unpublished GPS solutions. C. Beebe and N. Mietkiewicz contributed to graphical visualization of numerous models. Some of the ideas presented here were developed during proposal preparation with P. Haeussler, R. Bruhn, and P. Armstrong for which POK is grateful. Comprehensive and constructive reviews by A. Meigs and G. Plafker are greatly appreciated. This research has been generously funded by the Continental Dynamics Program of National Science Foundation (NSF EAR-CD STEEP-0409162) to Koons and EAR 0735402 Pavlis.

References

Abers, G. A., P. E. van Keken, E. A. Kneller, A. Ferris, and J. C. Stachnik (2006), The thermal structure of subduction zones constrained by seismic imaging: Implications for slab dehydration and wedge flow, *Earth Planet. Sci. Lett.*, *241*, 387–397, doi:10.1016/j.epsl.2005.11.055.

Bauer, M. A., G. L. Pavlis, M. Landes, and R. Hansen (2008), Crustal and lithospheric thickness variations for Central Alaska and the Chugach-St. Elias region from P and S receiver functions, *Eos Trans. AGU*, *89*(53), Fall Meet. Suppl., T53B-1945.

Berger, A. L., and J. A. Spotila (2008), Denudation and deformation in a glaciated orogenic wedge: The St. *Elias Orogen, Alaska, Geology*, *36*, 523–526, doi:10.1130/G24883A.1.

Berger, A. L., J. A. Spotila, J. B. Chapman, T. L. Pavlis, E. Enkelmann, N. A. Ruppert, and J. T. Buscher (2008a), Architecture, kinematics, and exhumation of a convergent orogenic wedge: A thermochronological investigation of tectonic-climatic interactions within the central St. Elias orogen, Alaska, *Earth Planet. Sci. Lett.*, *270*, 13–24, doi:10.1016/j.epsl.2008.02.034.

Berger, A. L., et al. (2008b), Quaternary tectonic response to intensified glacial erosion in an orogenic wedge, *Nat. Geosci.*, *1*, 793–799, doi:10.1038/ngeo334.

Billen, M. I., and G. Hirth (2006), Newtonian versus non-Newtonian upper mantle viscosity: Implications for subduction initiation, *Geophys. Res. Lett.*, *32*, L19304, doi:10.1029/2005GL023457.

Brace, W. F., and D. L. Kohlstedt (1980), Limits on lithospheric stress imposed by laboratory experiments, *J. Geophys. Res.*, *85*, 6248–6252, doi:10.1029/JB085iB11p06248.

Bruhn, R. L., and P. J. Haeussler (2006), Deformation driven by subduction and microplate collision: Geodyanmics of Cook Inlet basin, Alaska, *Geol. Soc. Am. Bull.*, *118*, 289–303, doi:10.1130/B25672.1.

Bruhn, R. L., T. Pavlis, G. Plafker, and L. Serpa (2004), Deformation during terrane accretion in the Saint Elias orogen, Alaska, *Geol. Soc. Am. Bull.*, *116*, 771–787, doi:10.1130/B25182.1.

Bruns, T. R. (1983), Model for the origin of the Yakutat Block, an accreted terrane in the northern Gulf of Alaska, *Geology*, *11*, 718–721, doi:10.1130/0091-7613(1983)11<718:MFTOOT>2.0.CO;2.

Buck, W. R., and A. N. B. Poliakov (1998), Abyssal hills formed by stretching oceanic lithosphere, *Nature*, *392*, 272–275, doi:10.1038/32636.

Chapman, J. B., et al. (2008), Neotectonics of the Yakutat collision: Changes in deformation driven by mass redistribution, in *Active Tectonics and Seismic Potential of Alaska*, *Geophys. Monogr. Ser. 179*, edited by J. T. Freymueller, P. J. Haeussler, R. Wesson, and G. Ekstrom, pp. 65–82, AGU, Washington, D. C.

Christeson, G. L., H. Van Avendonk, S. P. S. Gulick, L. Worthington, and T. Pavlis (2009), Crustal structure of the Yakutat Block: Constraints from STEEP wide-angle seismic data, *Geol. Soc. Abst.* w/Programs, 108–118.

Cundall, P., and M. Board (1988), A microcomputer program for modelling of large-strain plasticity problems, *Numerical Methods In Geomechanics*, *6*, 2101–2108.

DeMets, C., R. G. Gordon, D. F. Argus, and S. Stein (1994), Effect of recent revisions of geomagnetic reversal time-scale on estimate of current plate

motions, *Geophys. Res. Lett.*, *21*, 2191–2194, doi:10.1029/94GL02118.

Eberhart-Phillips, D., D. H. Christensen, T. M. Brocher, R. Hansen, N. A. Ruppert, P. J. Haeussler, and G. A. Aber (2006), Imaging the transition from Aleutian subduction to Yakutat collision in central Alaska, with local earthquakes and active source data, *J. Geophys. Res.*, *111*, B11303, doi:10.1029/2005JB004240.

Engebretson, D. C., A. Cox, and R. G. Gordon (1984), Relative motions between oceanic and continental plates in the Pacific basin, *Geol. Soc. Am. Special Paper 206*, 59 pp.

Enkelmann, E., J. I. Garver, and T. L. Pavlis (2008), Rapid exhumation of ice-covered rocks of the Chugach-St. Elias orogen, Southeast Alaska, *Geology*, *36*, 915–918, doi:10.1130/G2252A.1.

Enkelmann, E., P. K. Zeitler, T. L. Pavlis, J. I. Garver, and K. D. Ridgway (2009), Intense localized rock uplift and erosion in the St. Elias orogen of Alaska, *Nat. Geosci.*, *2*, 360–363, doi:10.1038/ngeo502.

Eyles, C. H., N. Eyles, and M. B. Lagoe (1991), The Yakataga Formation: A late Miocene to Pleistocene record of temperate glacial marine sedimentation in the Gulf of Alaska, in *Glacial-Marine Sedimentation; Paleoclimatic Significance*, *Geol. Soc. Am. Special Paper 261*, edited by J. B. Anderson and G. M. Ashley, pp. 159–180, Boulder, Colo.

Ferris, A., G. A. Abers, D. H. Christensen, and E. Veenstra (2003), High resolution image of the subducted Pacific (?) plate beneath central Alaska, 50–150 km depth, *Earth Planet. Sci. Lett.*, *214*, 575–588, doi:10.1016/S0012-821X(03)00403-5.

Fitzgerald, P. G., R. B. Sorkhabi, T. F. Redfield, and E. Stump (1995), Uplift and denudation of the central Alaska Range: A case study in the use of apatite fission-track thermochronology to determine absolute uplift parameters, *J. Geophys. Res.*, *100*, 20,175–20,191, doi:10.1029/95JB02150.

Fletcher, H. J., and J. T. Freymueller (1999), New GPS constraints on the motion of the Yakutat Block, *Geophys. Res. Lett.*, *26*, 3029–3032, doi:10.1029/1999GL005346.

Fletcher, H. J., and J. T. Freymueller (2003), New constraints on the motion of the Fairweather fault, Alaska, from GPS observations, *Geophys. Res. Lett.*, *30*(3), 1139, doi:10.1029/2002GL016476.

Fuis, G. S., et al. (2008), Trans-Alaska crustal transect and continental evolution involving subduction underplating and synchronous foreland thrusting, *Geology*, *36*, 267–270, doi:10.1130/G24257A.1.

Gulick, S. P. S., L. A. Lowe, T. L. Pavlis, J. V. Gardner, and L. A. Mayer (2008), Geophysical insights into Transition fault debate: Propagating strike-slip in response to stalling Yakutat block subduction in the Gulf of Alaska, *Geology*, *35*, 763–766, doi:10.1130/G23585A.1.

Hacker, B. R., G. A. Abers, and S. M. Peacock (2003), Subduction factory, 1, Theoretical mineralogy, densities, seismic wave speeds, and H_2O contents, *J. Geophys. Res.*, *108*(B1), 2029, doi:10.1029/2001JB001127.

Haeussler, P. J. (2008), An overview of the neotectonics of interior Alaska: Far-field deformation from the Yakutat microplate collision, in *Active Tectonics and Seismic Potential of Alaska*, *Geophys. Monogr. Ser*, vol. 179, edited by J. T. Freymueller, P. J. Haeussler, R. Wesson, and G. Ekstrom, pp. 83–108, AGU, Washington, D. C.

Haeussler, P. J., D. C. Bradley, and R. J. Goldfarb (2003), Brittle deformation along the Gulf of Alaska margin in response to Paleocene-Eocene triple junction migration, in *Geology of a Transpressional Orogen Developed during Ridge-Trench Interaction along the North Pacific Margin*: *Geol. Soc. Am. Special Paper 371*, edited by V. B. Sisson, S. M. Roeske, and T. L. Pavlis, pp. 119–140, Boulder, Colo., doi:10.1130/0-8137-2371-X.119.

Haeussler, P. J., P. O'Sullivan, A. L. Berger, and J. A. Spotila (2008), Neogene exhumation of the Tordrillo Mountains, Alaska, and correlations with Denali (Mt. McKinley), in *Active Tectonics and Seismic Potential of Alaska*, *Geophys. Monogr. Ser.* vol. 179, edited by J. T. Freymueller, P. J. Haeussler, R. Wesson, and G. Ekstrom, pp. 269–285, AGU, Washington, D. C.

Hallet, B., L. Hunter, and J. Bogen (1996), Rates of erosion and sediment evacuation by glaciers: A review of field data and their implications, *Global Planet. Change*, *12*, 213–235, doi:10.1016/0921-8181(95)00021-6.

Hirth, G., and J. Tullis (1992), Dislocation creep regimes in quartz aggregates, *J. Struct. Geol.*, *14*, 145–159, doi:10.1016/0191-8141(92)90053-Y.

Hobbs, B. E., H.-B. Mühlhaus, and A. Ord (1990), Instability, softening and localization of deformation, in *Deformation Mechanism, Rheology and Tectonics*, edited by R. J. Knipe and E. H. Rutter, *Geol. Soc. Spec. Pub. 54*, 143–165.

Itasca Consulting Group, Inc. (1997), FLAC3D (Fast Lagrangian Analysis of Continua in 3 Dimensions), Minneapolis, Minn.

Kalbas, J. L., K. D. Ridgway, and G. E. Gehrels (2007), Stratigraphy, depositional systems, and provenance of the Lower Cretaceous Kahiltna assemblage, western Alaska Range: Basin development in response to oblique collision, in *Tectonic Growth of a Collisional Continental Margin: Crustal Evolution of Southern Alaska*, *Geol. Soc. Am. Special Paper 431*, edited by K. D. Ridgway, J. M. Trop, J. M. G. Glen, and J. M. O'Neill, pp. 307–343, Boulder, Colo. doi:10.1130/2007.2431(20).

Kohlstedt, D. L., B. Evans, and S. J. Mackwell (1995), Strength of the lithosphere: Constraints imposed by laboratory experiments, *J. Geophys. Res.*, *100*, 17,587–17,602, doi:10.1029/95JB01460.

Koons, P. O. (1987), Some thermal and mechanical consequences of rapid uplift: An example from the Southern Alps, *Earth Planet. Sci. Lett.*, *86*, 307–319, doi:10.1016/0012-821X(87)90228-7.

Koons, P. O. (1990), Two-sided orogen: Collision and erosion for the sandbox to the Southern Alps, New Zealand, *Geology*, *18*, 679–682, doi:10.1130/0091-7613(1990)018<0679:TSOCAE>2.3.CO;2.

Koons, P. O. (1994), Three-dimensional critical wedges: Tectonics and topography in oblique collisional orogens, *J. Geophys. Res.*, *99*, 12,301–12,315, doi:10.1029/94JB00611.

Koons, P. O., and E. Kirby (2007), Topography, denudation, and deformation: The role of surface processes on fault evolution, in *Tectonic Faults: Agents of Change on a Dynamic Earth*, edited by M. R. Handy, G. Hirth, and N. Hovius, pp. 205–230, MIT Press, Cambridge, Mass.

Koons, P. O., P. K. Zeitler, C. P. Chamberlain, D. Craw, and A. S. Melzer (2002), Mechanical links between river erosion and metamorphism in Nanga Parbat, Pakistan Himalaya, *Am. J. Sci.*, *302*, 749–773, doi:10.2475/ajs.302.9.749.

Koons, P. O., R. J. Norris, D. Craw, and A. F. Cooper (2003), Influence of exhumation on the structural evolution of transpressional plate boundaries: An example from the Southern Alps, New Zealand, *Geology*, *31*, 3–6, doi:10.1130/0091-7613(2003)031<0003:IOEOTS>2.0.CO;2.

Lagoe, M. B., and S. D. Zellers (1996), Depositional and microfaunal response to Pliocene climate change and tectonics in the eastern Gulf of Alaska, *Mar. Micropaleontol.*, *27*, 121–140, doi:10.1016/0377-8398(95)00055-0.

Lagoe, M. B., C. H. Eyles, N. Eyles, and C. Hale (1993), Timing of late Cenozoic tidewater glaciation in the far North Pacific, *Geol. Soc. Am. Bull.*, *105*, 1542–1560, doi:10.1130/0016-7606(1993)105<1542:TOLCTG>2.3.CO;2.

Mackwell, S. J., M. E. Zimmerman, and D. E. Kohlstedt (1998), High temperature deformation of dry diabase with application to tectonics on Venus, *J. Geophys. Res.*, *103*, 975–984, doi:10.1029/97JB02671.

McAleer, R. J., J. A. Spotila, E. Enkelmann, and A. L. Berger (2009), Exhumation along the Fairweather fault, southeastern Alaska, based on low-temperature thermochronometry, *Tectonics*, *28*, TC1007, doi:10.1029/2007TC002240.

Meigs, A., and J. Sauber (2000), Southern Alaska as an example of the long-term consequences of mountain building under the influence of glaciers, *Quat. Sci. Rev.*, *19*, 1543–1562, doi:10.1016/S0277-3791(00)00077-9.

Meigs, A., S. Johnston, J. Garver, and J. Spotila (2008), Crustal-scale structural architecture, shortening, and exhumation of an active, eroding orogenic wedge (Chugach/St. Elias Range, southern Alaska), *Tectonics*, *27*, TC4003, doi:10.1029/2007TC002168.

Miller, M. L., D. C. Bradley, T. K. Bundtzen, and W. McClelland (2002), Late Cretaceous through Cenozoic strike-slip tectonics of southwestern Alaska, *J. Geol.*, *110*, 247270, doi:10.1086/339531.

Montési, G. J. L., and M. T. Zuber (2002), A unified description of localization for application to large-scale tectonics, *J. Geophys. Res.*, *107*(B3), 2045, doi:10.1029/2001JB000465.

Nokleberg, W. J., G. Plafker, and F. H. Wilson (1994), Geology of south-central Alaska, in *The Geology of North America, v. G-1*, *The Geology of Alaska*, edited by G. Plafker and H. C. Berg, pp. 311–366, Geol. Soc. Am., Boulder, Colo.

O'Sullivan, P. B., and L. D. Currie (1996), Thermotectonic history of Mt Logan, Yukon Territory, Canada; implications of multiple episodes of middle to late Cenozoic, *Earth Planet. Sci. Lett.*, *144*, 251–261, doi:10.1016/0012-821X(96)00161-6.

Pavlis, T. L., and R. L. Bruhn (1983), Deep-seated flow as a mechanism for the uplift of broad forearc ridges and its role in the exposure of high P/T metamorphic terranes, *Tectonics*, *2*, 473–497, doi:10.1029/TC002i005p00473.

Pavlis, T. L., and V. B. Sisson (2003), Development of a subhorizontal decoupling horizon in a transpressional system, Chugach metamorphic complex, Alaska: Evidence for rheological stratification of the crust, in *Geology of a transpressional orogen developed during ridge-trench interaction along the North Pacific margin*, *Geol. Soc. Am. Special Paper 371*, edited by V. B. Sisson, S. M. Roeske, and T. L. Pavlis, pp. 191–216.

Pavlis, G. L., C. Picornell, L. Serpa, R. L. Bruhn, and G. Plafker (2004), Tectonic processes during oblique collision: Insights from the St. Elias orogen, northern North American Cordillera, *Tectonics*, *23*, TC3001, doi:10.1029/2003TC001557.

Péwé, T. L. (1975), Quaternary geology of Alaska, *U.S. Geol. Surv. Prof. Pap.*, *835*, 145 pp.

Plafker, G. (1965), Tectonic deformation associated with the 1964 Alaska earthquake, *Science*, *148*, 1675–1687, doi:10.1126/science.148.3678.1675.

Plafker, G. (1987), Regional geology and petroleum potential of the northern Gulf of Alaska continental margin, in *Geology and Resource Potential of the Continental Margin of Western North America and Adjacent Ocean Basins*, Circum-Pacific Council for Energy and Mineral Resources, Earth Science Series, vol. 6, edited by D. W. Scholl, A. Grantz, and J. G. Vedder, pp. 229–268, Circum-Pacific Council for Energy and Mineral Resources, Houston, Tex.

Plafker, G. L. M. Gilpen L.M., and J. C. Lahr (1994b), Neotectonic map of Alaska, in *The Geology of North America, v. G-1*, *The Geology of Alaska*, edited by G. Plafker and H. C. Berg, 1 sheet, scale 1:2,500,000, Geol. Soc. Am., Boulder, Colo.

Plafker, G., and H. C. Berg (1994), Overview of the geology and tectonic evolution of Alaska, in *The Geology of North America, v. G-1*, *The Geology of Alaska*, edited by G. Plafker and H. C. Berg, pp. 989–1021, Geol. Soc. Am., Boulder, Colo.

Plafker, G., T. Hudson, T. R. Bruns, and M. Rubin (1978), Late Quaternary offsets along the Fairweather Fault and crustal plate interactions in southern Alaska, *Can. J. Earth Sci.*, *15*, 805–816.

Plafker, G., J. C. Moore, and G. R. Winkler (1994a), Geology of the southern Alaska margin, in *The Geology of North America, v. G-1*, *The Geology of Alaska*, edited by G. Plafker and H. C. Berg, pp. 389–449, Geol. Soc. Am., Boulder, Colo.

Preece, S. J., and W. K. Hart (2004), Geochemical variations in the <5 Ma Wrangell Volcanic Field, Alaska: Implications for the magmatic and tectonic development of a complex continental arc system, *Tectonophysics*, *392*, 165–191, doi:10.1016/j.tecto.2004.04.011.

Redfield, T. F., D. W. Scholl, P. G. Fitzgerald, and M. E. Beck Jr. (2007), Escape tectonics and the extrusion of Alaska: Past, present, and future, *Geology*, *35*, 1039–1042, doi:10.1130/G23799A.1.

Ridgway, K. D., E. E. Thoms, P. W. Layer, M. E. Lash, J. M. White, and S. V. Smith (2007) Neogene transpressional foreland basin development on the north side of the central Alaska Range, Usibelli Group and Nenana Gravel, Tanana basin, in *Tectonic Growth of a Collisional Continental Margin: Crustal Evolution of Southern Alaska*, *Geol. Soc. Am. Special Paper 431*, edited by K. D. Ridgway, J. M. Trop, J. M. G. Glen, and J. M. O'Neill, pp. 507–547, Boulder, Colo. doi: 10.1130/2007.2431(20).

Scholl, D. W., A. J. Stevenson, S. Mueller, E. L. Geist, D. C. Engebretson, and T. L. Vallier (1992), Exploring the notion that southeast-Asian-type escape tectonics and trench clogging are involved in regional-scale deformation of Alaska and the formation of the Aleutian-Bering Sea region, in *Southeast Asia Structure, Tectonics, and Magmatism*, *Proc. Geodynamics Res. Inst, Symp.*, edited by M. Flower, R. McCabe, and T. Hilde, pp. 57–63, Texas A&M Univ., College Station, Tex.

Smith, A. J., R. D. Hydman, J. F. Cassidy, and K. Wang (2003), Structure, seismicity and thermal regime of the Queen Charlotte transform margin, *J. Geophys. Res.*, *108*(B11), 2539, doi:10.1029/2002JB002247.

Stout, J. H., and C. G. Chase (1980), Plate kinematics of the Denali fault system, *Can. J. Earth Sci.*, *17*, 1527–1537.

Upton, P., P. O. Koons, and D. Eberhart-Phillips (2003), Extension and partitioning in an oblique subduction zone, New Zealand: Constraints from three-dimensional numerical modeling, *Tectonics*, *22*(6), 1068, doi:10.1029/2002TC001431.

Upton, P., K. Mueller, and Y.-G. Chen (2009), 3D numerical models with varied material properties and erosion rates: Implications for the mechanics and kinematics of compressive wedges, *J. Geophys. Res.*, *114*, B04408, doi:10.1029/2008JB005708.

Vermeer, P. A., and R. de Borst (1984), Non-associated plasticity for soils, concrete, and rock, *Heron*, *29*, 3–64.

von Huene, R., and D. W. Scholl (1991), Observations at convergent margins concerning sediment subduction, subduction erosion, and the growth of continental crust, *Rev. Geophys.*, *29*, 279–316, doi:10.1029/91RG00969.

Whipple, K. X., and B. J. Meade (2006), Orogen response to changes in climatic and tectonic forcing, *Earth Planet. Sci. Lett.*, *243*, pp. 218–228.

Willett, S. D., C. Beaumont, and P. Fullsack (1993), Mechanical model for the tectonics of doubly vergent compressional orogens, *Geology*, *21*, pp. 371–374.

Wijns, C., R. Weinberg, K. Gessner, and L. Moresi (2005), Mode of crustal extension determined by rheological layering, *Earth Planet. Sci. Lett.*, *236*(1–2), 120–134, doi:10.1016/j.epsl.2005.05.030.

Worthington, L. L., G. L. Christeson, H. J. Van Avendonk, and S. P. Gulick (2009), Crustal structure of the Yakutat Microplate: New parameters for understanding the evolution of the Chugach-St. Elias Orogeny, *Eos Trans. AGU*, *90*(52), Fall Meet. Suppl., T53F-03.

Zeitler, P. K., et al. (2001), Crustal Reworking at Nanga Parbat, Pakistan: Evidence for erosional focusing of crustal strain, *Tectonics*, *20*, 712–728, doi:10.1029/2000TC001243.

Zellers, S. D. (1995), Foraminiferal sequence biostratigraphy and seismic stratigraphy of a tectonically active margin: The Yakataga Formation, northeastern Gulf of Alaska, *Mar. Micropaleontol.*, *26*, 255–271, doi:10.1016/0377-8398(95)00031-3.

A. D. Barker, Department of Earth and Space Sciences, University of Washington, Johnson Hall 070, Box 351310, Seattle, WA 98195, USA.

B. P. Hooks and T. Pavlis, Department of Geological Science, University of Texas at El Paso, 500 West University Boulevard, El Paso, TX 79968, USA. (bphooks@utep.edu)

P. O. Koons, Department of Earth Sciences/Climate Change Institute, University of Maine, Bryand Global Sciences Center, Orono, ME 04469, USA.

P. Upton, GNS Science, Dunedin Research Centre, 764 Cumberland St, Dunedin, Private Bag 1930, Dunedin 9054, New Zealand.